Conditional Sampling in a Transitional Boundary Layer Under High Freestream Turbulence Conditions

Ralph J. Volino
e-mail: volino@usna.edu

Michael P. Schultz

Christopher M. Pratt

Department of Mechanical Engineering,
United States Naval Academy,
Annapolis, MD 21402

Conditional sampling has been performed on data from a transitional boundary layer subject to high (initially 9%) freestream turbulence and strong ($K=(\nu/U_\infty^2)(dU_\infty/dx)$ *as high as* 9×10^{-6}) *acceleration. Methods for separating the turbulent and nonturbulent zone data based on the instantaneous streamwise velocity and the turbulent shear stress were tested and found to agree. Mean velocity profiles were clearly different in the turbulent and nonturbulent zones, and skin friction coefficients were as much as 70% higher in the turbulent zone. The streamwise fluctuating velocity, in contrast, was only about 10% higher in the turbulent zone. Turbulent shear stress differed by an order of magnitude, and eddy viscosity was three to four times higher in the turbulent zone. Eddy transport in the nonturbulent zone was still significant, however, and the nonturbulent zone did not behave like a laminar boundary layer. Within each of the two zones there was considerable self-similarity from the beginning to the end of transition. This may prove useful for future modeling efforts.* [DOI: 10.1115/1.1521957]

Introduction

Boundary layer transition is an important phenomenon experienced by the flow through gas turbine engines. Mayle [1] stated that a substantial fraction of the boundary layer on both sides of a gas turbine airfoil may be transitional. The extended transition zones exist due to strong favorable pressure gradients, found on both the pressure side and the leading section of the suction side, which stabilize the boundary layer and delay transition in spite of the high freestream turbulence intensity (FSTI) in gas turbine environments. The ability to model and predict high FSTI transition is important since heat transfer rates and skin friction coefficients may increase substantially when a boundary layer undergoes transition. Boundary layer separation, which is believed to be a significant problem on the suction side of some low-pressure turbine airfoils, also depends strongly on the state of the boundary layer with respect to transition. Improved transition models and turbine designs depend, therefore, on a better understanding of high FSTI transition.

Documentation of high FSTI transition has included work in turbine cascades and rotating rigs (e.g., Halstead et al. [2]). Several studies have considered the flow along flat and curved walls. These simpler geometries allow for more detailed in-flow measurements than are typical for cascade studies. On surfaces subject to zero streamwise pressure gradients, Blair [3], Sohn and Reshotko [4], and Kim et al. [5] all showed that at FSTI above about 3%, transition occurred rapidly near the leading edge of a test surface. Blair [6] considered cases with FSTI up to 5% and concurrent acceleration, holding the acceleration parameter, K, constant at values up to 0.75×10^{-6}. The acceleration delayed the transition, even with high FSTI. Volino and Simon [7–9] considered transition along a concave wall with inlet FSTI of 8% and acceleration with K as high as 9×10^{-6}. Acceleration rates, Reynolds numbers and FSTI were typical of the pressure side of a gas turbine airfoil. An extended transition region, with intermittent turbulent and nonturbulent zones, covered most of the test surface. The turbulent zone included a range of both large and small scale eddies, much like a fully turbulent boundary layer and the turbulent zone in a low FSTI transitional boundary layer. The nonturbulent zone and the pre-transitional boundary layer were not laminar-like as in a low FSTI flow, but instead were characterized by high-amplitude large-scale fluctuations and an absence of smaller scales. Nonturbulent zone velocity fluctuations are believed to be induced by the freestream unsteadiness through pressure fluctuations, as discussed in Volino [10]. Near-wall turbulence production is believed to be largely absent in the nonturbulent zone.

The intermittent nature of transition, both at low and high FSTI, has led to efforts to incorporate intermittency in transition models and to model the two zones of the intermittent flow separately. Among recent efforts are the work of Steelant and Dick [11], Suzen and Huang [12], and Solomon et al. [13]. Separate modeling of the nonturbulent and turbulent zones requires knowledge of the flow behavior within each zone, which can be provided through conditional sampling of experimental data. Conditional sampling results have been presented for zero streamwise pressure gradient conditions by Kim et al. [5], Sohn and Reshotko [4], and Kuan and Wang [14]. Results from favorable pressure gradient cases have been reported by Blair [6], Wang and Keller [15], and Wang and Zhou [16]. The strongest acceleration rate in these cases was $K=0.75\times10^{-6}$. This is a relatively mild acceleration for modern airfoils, and the transition zones were short in all cases with elevated FSTI.

Volino and Simon [7,9] obtained rough estimates of the time-averaged intermittency (fraction of time the flow is turbulent) in their high FSTI, strong acceleration case using an analog circuit, which determined when the flow was turbulent based on the time derivatives of hot-wire voltages. The circuit worked well in the low FSTI cases of Kim et al. [5], but in high FSTI cases differences in fluctuation level between the turbulent and nonturbulent zones are narrower, and more careful setting of thresholds and smoothing of the intermittency function are required for conditional sampling. This is difficult with an analog circuit, and is better done in post-processing after the signal has been digitized. Such post-processing requires data acquisition at a high enough sampling rate to provide an essentially continuous signal. Due to

Contributed by the Fluids Engineering Division for publication in the JOURNAL OF FLUIDS ENGINEERING. Manuscript received by the Fluids Engineering Division July 12, 2001, revised manuscript received July 26, 2002. Associate Editor: K. B. M. Q. Zaman.

Report Documentation Page

Form Approved
OMB No. 0704-0188

1. REPORT DATE	2. REPORT TYPE	3. DATES COVERED
JUL 2002		**00-00-2002 to 00-00-2002**

4. TITLE AND SUBTITLE	5a. CONTRACT NUMBER
Conditional Sampling in a Transitional Boundary Layer Under High Freestream Turbulence Conditions	5b. GRANT NUMBER
	5c. PROGRAM ELEMENT NUMBER
6. AUTHOR(S)	5d. PROJECT NUMBER
	5e. TASK NUMBER
	5f. WORK UNIT NUMBER
7. PERFORMING ORGANIZATION NAME(S) AND ADDRESS(ES) **United States Naval Academy,Department of Mechanical Engineering,Annapolis,MD,21402**	8. PERFORMING ORGANIZATION REPORT NUMBER
9. SPONSORING/MONITORING AGENCY NAME(S) AND ADDRESS(ES)	10. SPONSOR/MONITOR'S ACRONYM(S)
	11. SPONSOR/MONITOR'S REPORT NUMBER(S)

12. DISTRIBUTION/AVAILABILITY STATEMENT
Approved for public release; distribution unlimited

13. SUPPLEMENTARY NOTES

14. ABSTRACT

15. SUBJECT TERMS

16. SECURITY CLASSIFICATION OF:			17. LIMITATION OF ABSTRACT	18. NUMBER OF PAGES	19a. NAME OF RESPONSIBLE PERSON
a. REPORT **unclassified**	b. ABSTRACT **unclassified**	c. THIS PAGE **unclassified**	**Same as Report (SAR)**	**10**	

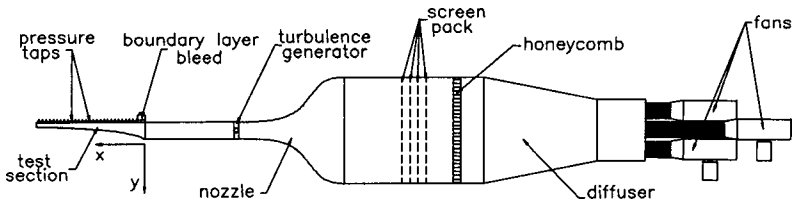

Fig. 1 Schematic of the test facility

data storage limitations at the time, Volino and Simon [7,9] only sampled at a high enough rate for such processing at a few isolated points in the boundary layer. Volino [17] examined the data from these points using wavelet analysis and presented preliminary results of conditional sampling. Uncertainties were high due to the limited amount of data. To the authors' knowledge, no other detailed conditional sampling results from boundary layers with strong acceleration, extended transition zones and FSTI greater than 5% are available in the literature.

The present paper has two objectives. The first is to provide the results of conditional sampling for a transitional boundary layer with high FSTI and strong acceleration. The case presented by Volino and Simon [7–9] has been reproduced on a flat test wall, and data have been acquired throughout the boundary layer at a sufficiently high sampling rate for conditional sampling post processing. The second objective is to provide a baseline case for a study of the significance of streamwise curvature on transitional boundary layers at elevated FSTI. A second paper (Schultz and Volino [18]) presents results from an otherwise similar case on a wall with strong concave curvature.

Experiments

Facility and Measurements. All experiments were conducted in the low speed wind tunnel shown in Fig. 1. Three fans supply air to a plenum, which is followed by a diffuser, a settling chamber containing a honeycomb, a screen pack, a second settling chamber, and a three-dimensional contraction which reduces the cross sectional area from 1.09 m×1.09 m to 0.69 m×0.18 m. A bi-planar turbulence-generating grid with 43% blockage is in the plane of the contraction exit. The grid is based on the design used by Kim et al. [5] and consists of a 3.8-cm diameter, 0.69-m long vertical pipe down the center of the contraction exit, and six 3.2-cm diameter, 0.18-m long evenly spaced horizontal pipes. Following the grid is a 1-m long rectangular development section and the test section, a converging channel. One side of this channel is a flat Plexiglas plate of 0.69 m width and 1.2 m length, which serves as the test wall. Pressure taps are installed along its spanwise centerline. At the leading edge of the test wall a slot is used to bleed off the boundary layer which grows in the development section. Opposite the test wall is a flexible wall which can be adjusted to set the desired pressure gradient along the test wall. For the present study the inlet velocity is set to 4.6 m/s and the velocity gradient along the wall is held constant at 13.9 s^{-1}. The acceleration parameter, K, drops from a maximum of 9×10^{-6} at the inlet to the test section to 1×10^{-6} at the last measurement station. Values of K through the test section, measurement locations and other parameters are given in Table 1.

At the inlet to the test section the mean flow is spatially uniform to within 3% and the turbulence is uniform to within 6%. The components of the freestream turbulence intensity are 8.8%, 8.9%, and 8.3% in the streamwise, cross-stream, and spanwise directions, respectively. The integral length scales of these components of the freestream turbulence are 3 cm, 1.6 cm, and 1.4 cm. Spectra of the freestream turbulence at the most upstream measurement station are shown in Fig. 2. In the test section, the freestream turbulence intensity (normalized using the local freestream velocity) drops to about 2% at the last measurement station. The drop is primarily due to the increasing freestream velocity. The streamwise component $\overline{u'_\infty}$ does decay somewhat due to straining of the freestream eddies in the accelerating flow, but $\overline{v'_\infty}$ remains nearly constant at all stations.

Velocity profile measurements were made at ten streamwise stations along the centerline of the test wall using a single sensor,

Table 1 Flow parameters at measurement stations

St	x [m]	U_∞ [m/s]	$\frac{\overline{u'_\infty}}{U_\infty}$ [%]	$\frac{\overline{v'_\infty}}{U_\infty}$ [%]	K $\times10^6$	γ_{pk} [%]	$\delta_{99.5}$ [mm]	Re_x $\times10^{-5}$
1	0.118	6.22	6.4	6.4	5.32	4.1	4.04	0.50
2	0.190	7.12	4.9	5.5	4.04	3.0	3.99	0.91
3	0.268	7.99	3.9	4.8	3.25	4.7	4.52	1.43
4	0.345	9.13	3.2	4.2	2.53	8.9	5.16	2.07
5	0.423	10.4	2.7	3.8	1.97	17.	4.72	2.88
6	0.503	11.4	2.4	3.4	1.63	34.	5.28	3.77
7	0.581	12.5	2.1	3.2	1.33	56.	5.67	4.84
8	0.659	13.6	1.9	2.9	1.13	71.	5.80	5.91
9	0.735	14.6	1.7	2.7	0.97	86.	6.58	7.20
10	0.817	15.9	1.5	2.5	0.83	93.	7.92	8.54

St	Re_θ	H	C_f $\times10^3$	Re_θ	H	C_f $\times10^3$	Re_θ	H	C_f $\times10^3$
	composite			non-turbulent			turbulent		
1	136	1.96	6.50	136	1.97	6.50	90	1.97	10.5
2	149	1.98	5.75	149	1.99	5.75	135	1.72	9.60
3	169	1.94	5.35	168	1.94	5.40	186	1.59	8.90
4	196	1.87	5.00	193	1.89	5.00	244	1.51	8.10
5	221	1.82	4.80	212	1.86	4.70	293	1.48	7.50
6	263	1.76	4.50	239	1.86	4.20	366	1.46	6.70
7	324	1.66	4.60	264	1.86	4.00	432	1.46	6.10
8	372	1.58	5.00	278	1.82	4.10	474	1.43	6.10
9	457	1.49	5.30	297	1.81	3.90	580	1.39	5.90
10	580	1.43	5.60	364	1.69	3.70	745	1.35	5.50

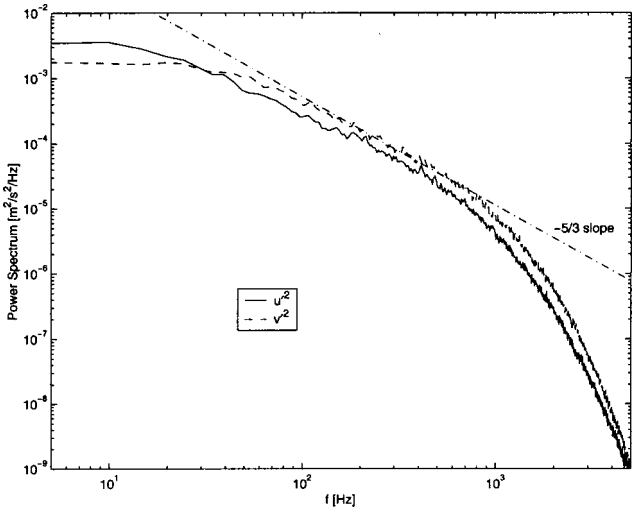

Fig. 2 Freestream spectra at Station 1

boundary layer type hot-wire probe (TSI model 1218-T1.5), a boundary layer cross-wire probe (TSI model 1243-T1.5), and a constant-temperature hot-wire anemometer (TSI model IFA-100). The probes were moved normal to the wall at each station using a motorized traverse with minimum step size of 12.5 μm. At each position in the velocity profiles, data were acquired for 26 seconds at a 20 kHz sampling rate (2^{19} data points). The hot-wire signals were low-pass filtered at 10 kHz. All raw data were stored. Sampling at 20 kHz provided essentially continuous velocity traces for subsequent processing.

Data Processing. Mean and rms fluctuating velocities in the streamwise and wall-normal directions were computed from the instantaneous data. Uncertainties in these quantities are 3–5% except in the very near wall region ($y^+<5$) where near-wall corrections (Wills [19]) are applied to the mean velocity. Uncertainty in the turbulent shear stress, $-\overline{u'v'}$, is 10%. Skin friction coefficients were determined using a technique whereby τ_w was adjusted until the U^+ versus y^+ data fit profiles computed using near-wall similarity, as described by Volino and Simon [20]. This technique accounts for pressure gradient effects on the near wall profile. Uncertainty in C_f is 8%. Boundary layer thicknesses were determined from the mean velocity profiles. Uncertainties in the momentum and displacement thicknesses are 10%. These uncertainties include bias uncertainties which tend to cancel such that the uncertainty in the shape factor, H, is 7%.

Intermittency Based on u. The intermittency function, Γ, indicates whether the boundary layer is instantaneously turbulent or nonturbulent at a measurement location. It is assigned a value of zero for nonturbulent flow and one for turbulent flow. The time average of Γ is the intermittency, γ. Keller and Wang [21] and Solomon [22] review several techniques for determining Γ. In the present study, two intermittency detection techniques were utilized and compared. The first, as used in Volino and Hultgren [23], is based on the instantaneous streamwise velocity, u. The u signal is first digitally high-pass filtered with a cutoff frequency

$$f_{HP}=200\cdot U_\infty \tag{1}$$

where f_{HP} is in Hz and U_∞ is in m/s. The filter eliminates low-frequency fluctuations, which are common to both the turbulent and nonturbulent zones. The filter was used by Volino and Hultgren [23] to remove narrow band fluctuations associated with shear layer instabilities in separated boundary layers. In the present work, this filter had little effect on the intermittency function. The filtered signal is then used to determine an intermittency function Γ_{1u}, as

$$\Gamma_{1u}(t)=\begin{matrix}1 & \text{if } |\partial u/\partial t|>8.89\cdot U_m\cdot U_\infty\\ 0 & \text{otherwise}\end{matrix} \tag{2}$$

where

$$U_m=\begin{matrix}U+2\cdot\overline{u'^3}^{1/3}-\overline{u'^2}^{1/2} & \text{if } 2\cdot\overline{u'^3}^{1/3}>\overline{u'^2}^{1/2}\\ U & \text{otherwise}\end{matrix} \tag{3}$$

The velocity U is the local mean velocity at the measurement location and U_∞ is the local freestream velocity at the measurement station. All velocities are in m/s, and the time derivative is in m/s^2. The time derivative of the velocity should scale with the magnitude of the velocity and the frequency with which eddies pass, which in turn also scales with the velocity. This explains the velocity squared term in the threshold in Eq. (2). The use of U_m instead of U_∞ allowed the threshold level to adjust in the near-wall region where the mean velocity becomes small. Very near the wall, as U approaches zero, the threshold would also approach zero and Γ_{1u} would go to 1 if U_m were set equal to U. To prevent this, U_m is adjusted using the fluctuating velocity, as shown in Eq. (3). This adjustment models the instantaneous rise in the near wall velocity which occurs during turbulent intervals when higher speed fluid sweeps toward the wall.

A second function, Γ_{2u}, is next computed based on the absolute value of the second derivative of the filtered velocity signal, $|\partial^2 u/\partial t^2|$. The threshold for Γ_{2u} is set such that the time average of Γ_{1u} and Γ_{2u} are equal. Next, a combined intermittency function, Γ_{3u} is defined as

$$\Gamma_{3u}(t)=\begin{matrix}1 & \text{if } \Gamma_1=1 \text{ or } \Gamma_2=1\\ 0 & \text{otherwise}\end{matrix} \tag{4}$$

Basing Γ_{3u} on both the first and second time derivative of the velocity helps to minimize dropouts within the turbulent zone, which occur in Γ_{1u} and Γ_{2u} when the derivatives cross zero. The final step is to smooth Γ_{3u} to minimize false turbulent points in the nonturbulent zone and false nonturbulent points in the turbulent zone. The function Γ_{3u} is low-pass filtered with cutoff frequency

$$f_{LP}=17.78\cdot U_\infty \tag{5}$$

where f_{LP} is in Hz and U_∞ is in m/s. Finally, using the filtered Γ_{3u}, the intermittency function Γ_u is set as

$$\Gamma_u(t)=\begin{matrix}1 & \text{if } \Gamma_{3u}>0.5\\ 0 & \text{otherwise}\end{matrix} \tag{6}$$

The thresholds and filter frequencies presented above were set after visual inspection of many data traces and the $\Gamma_u(t)$ resulting with several different thresholds. Visual inspection of the data is ultimately the best criteria available for determining how well an intermittency function is separating the turbulent and nonturbulent flow [17,22]. The thresholds and frequencies were useful both for the present study and the separated flow transition study of Volino and Hultgren [23]. They are not expected to be universal criteria for all flows, and other intermittency detection schemes might work as well. The thresholds might be made more general if nondimensionalized using the viscosity or a characteristic length such as the boundary layer thickness.

Intermittency Based on $u'v'$. A second intermittency function is computed based on the instantaneous turbulent shear stress. Without pre-filtering of the velocity signal, an intermittency function is computed as

$$\Gamma_{1uv}(t)=\begin{matrix}1 & \text{if } (\partial u'v'/\partial t)^2>50\cdot U_\infty^4\\ 0 & \text{otherwise}\end{matrix} \tag{7}$$

A second function Γ_{2uv} is computed based on $(\partial^2 u'v'/\partial t^2)^2$ with the threshold set such that the time averages of Γ_{1uv} and Γ_{2uv} are

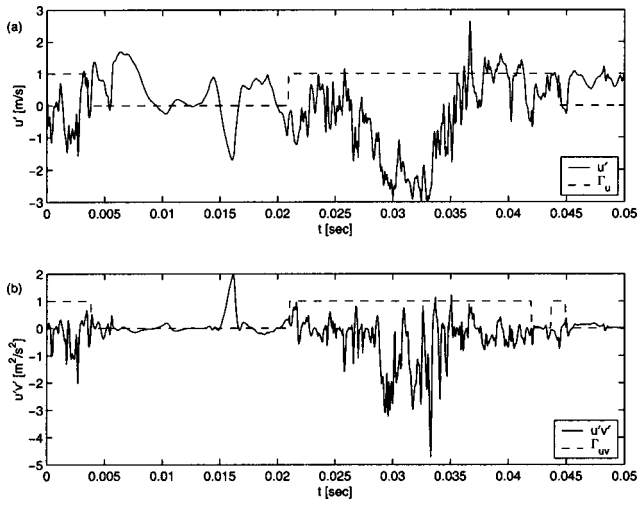

Fig. 3 Instantaneous velocity traces and intermittency function: (*a*) u and Γ_u, (*b*) $u'v'$ and Γ_{uv}

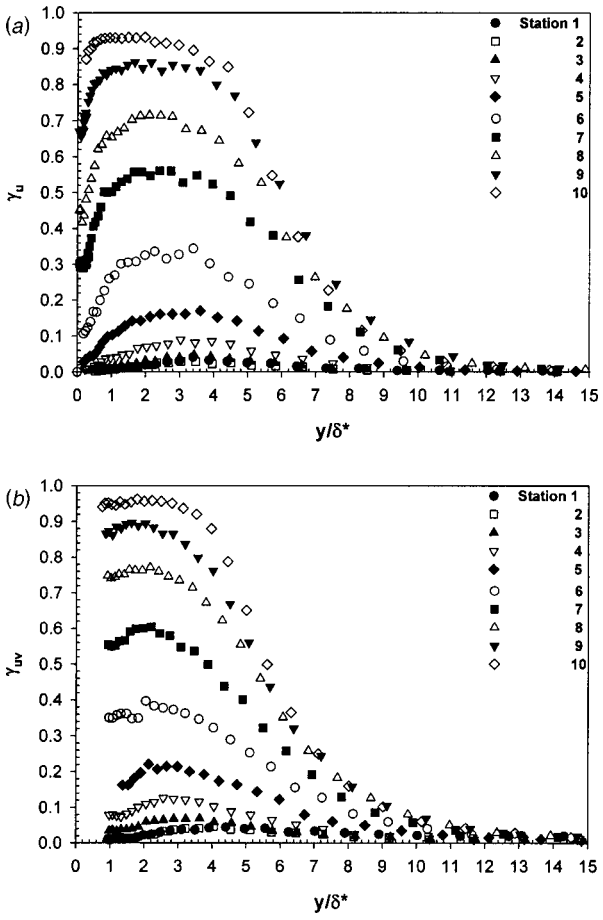

Fig. 4 Intermittency profiles based on (*a*) u and (*b*) Reynolds shear stress

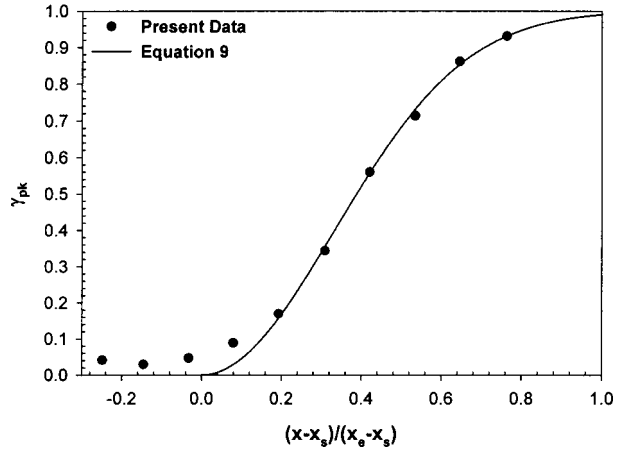

Fig. 5 Peak intermittency in profile versus dimensionless streamwise location

equal. The remaining steps in computing the intermittency function $\Gamma_{uv}(t)$ follow the steps in Eqs. (4)–(6) above.

Figure 3 presents a typical signal from the transitional boundary layer along with both intermittency functions. Some regions are clearly turbulent (e.g., 0.025 s–0.035 s) and some are clearly nonturbulent (0.01 s–0.02 s). Between zones the demarcation is not always sharp (0.04 s–0.045 s) leading to differences in $\Gamma_u(t)$ and $\Gamma_{uv}(t)$ and the possibility of some ''leakage'' of data between zones. The correlation coefficient between $\Gamma_u(t)$ and $\Gamma_{uv}(t)$ was always at least 0.8, however, and at 95% of the measurement locations it was above 0.9. Although the shear stress is often considered a better criterion function, the good agreement between $\Gamma_u(t)$ and $\Gamma_{uv}(t)$ suggest that both are acceptable. This is particularly useful very near the wall, where only u can be measured. Both functions were used in conditional sampling, providing essentially the same results. The uncertainty in the intermittency, γ, is 0.1. In the figures which follow, data points are shown for the nonturbulent zone only when the local $\gamma<95\%$, and for the tur-

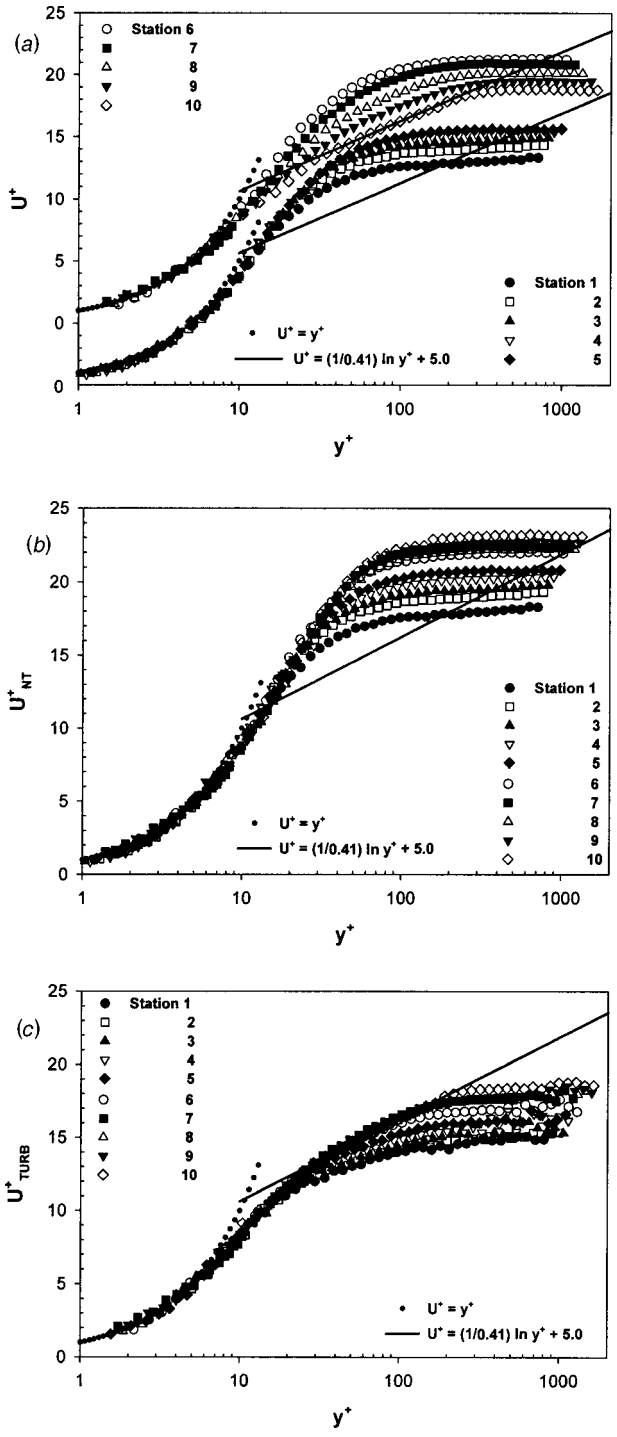

Fig. 6 Mean velocity profiles in wall coordinates: (*a*) composite; (*b*) nonturbulent; (*c*) turbulent

bulent zone only when $\gamma > 5\%$. Bulk parameters such as C_f are presented when $\gamma_{pk} < 95\%$ and $\gamma_{pk} > 5\%$ for the nonturbulent and turbulent zones, respectively.

Results

Intermittency. Intermittency profiles for the ten measurement stations are shown in Fig. 4. Agreement between the u and shear stress based γ is good. Intermittency remains low for the first three stations and then begins to rise. By the last station, transition is nearing completion. Transition criteria such as those presented by Johnson [24] and Mayle [1] indicate that the present boundary layer would be transitional by Station 1 under zero pressure gradient conditions. In fact, the intermittency is nonzero at Station 1, but the strong acceleration prevents the transition from proceeding. The beginning of the rise in γ corresponds to K dropping below 3×10^{-6}. In low FSTI boundary layers, $K>3\times10^{-6}$ leads to relaminarization (Jones and Launder [25]). Following the technique of Narasimha [26], as modified by Volino and Simon [27], the function

$$f(\gamma_{pk}) = (-\ln(1-\gamma_{pk}))^{1/2} \tag{8}$$

can be computed based on the peak intermittency at each station and plotted versus streamwise location. The data in these coordinates tend to lie along a straight line. The line may be extrapolated to $f(\gamma_{pk}=0)=0$ and $f(\gamma_{pk}=0.99)=2.146$, corresponding to the beginning and end of transition at $x_s=0.29$ m and $x_e=0.98$ m, respectively. Figure 5 shows γ_{pk} plotted versus dimensionless streamwise location within transition. Also shown is the theoretical curve

$$\gamma_{pk} = \exp\left(-4.6\left(\frac{x-x_s}{x_e-x_s}\right)^2\right) \tag{9}$$

based on the Dhawan and Narasimha [28] transition model. Agreement between the data and theory is good. In favorable pressure gradients some differences are expected and observed at low intermittency, in a region Narasimha [26] referred to as "subtransition."

The dimensionless turbulent spot propagation rate may be computed, following the development of Mayle [1], as

$$\hat{n}\sigma = \frac{4.6\nu^2\overline{U}_\infty}{(x_e-x_s)^2U_s^3} \tag{10}$$

where $\overline{U}_\infty$ is the average freestream velocity in the transition region. In the present case $\hat{n}\sigma=4.2\times10^{-11}$. In agreement with trends reported by Mayle [1] for other favorable pressure gradient cases, this value is an order of magnitude lower than what would be expected for a zero-pressure gradient case with the same FSTI, indicating a longer transition zone with the favorable pressure gradient than with a zero-pressure gradient.

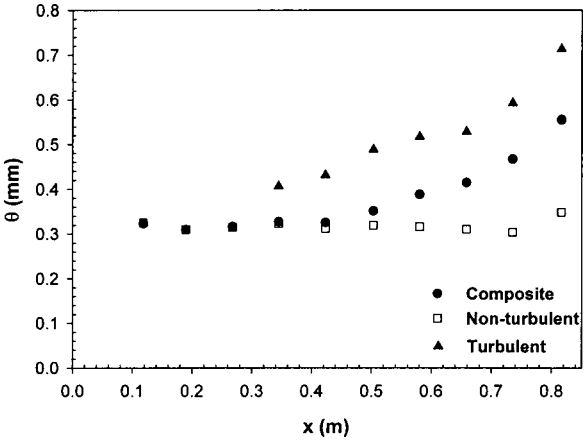

Fig. 8 Momentum thickness versus streamwise distance

Mean Velocity Profiles. Mean velocity profiles for the ten measurement stations are presented in Fig. 6 in wall coordinates. Figure 6(*a*) shows the composite (unconditioned) profiles. The profiles rise through Station 6, with a somewhat laminar-like shape. Downstream of Station 6, the profiles assume a more turbulent-like shape and by Station 10, where transition is near completion and the acceleration rate has dropped to $K=1$

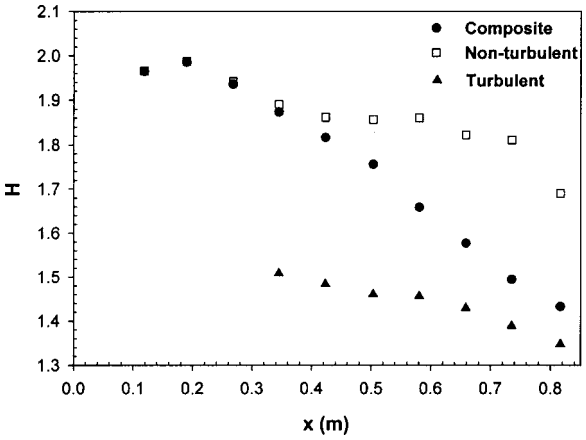

Fig. 9 Shape factor versus streamwise distance

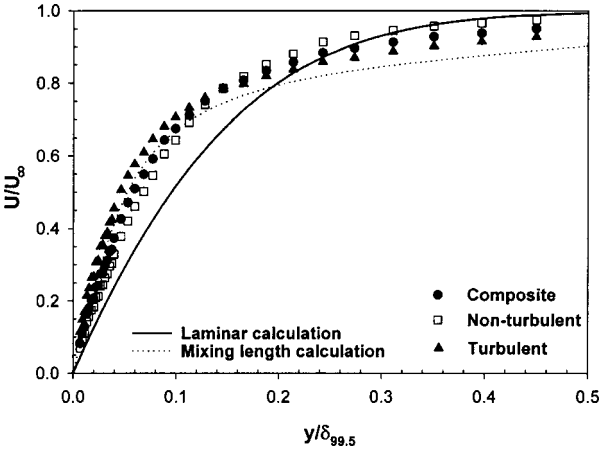

Fig. 7 Mean velocity profile for Station 7, $\gamma_{pk}=56\%$

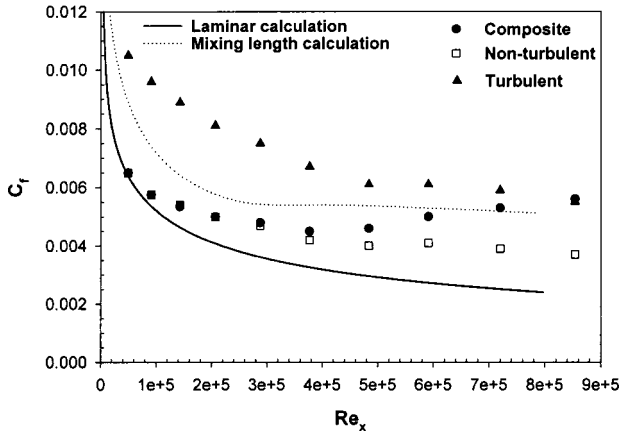

Fig. 10 Skin-friction coefficient

$\times 10^{-6}$, there is good agreement with the zero pressure gradient law of the wall. The nonturbulent zone profiles are shown in Fig. 6(*b*). All the profiles exhibit a laminar-like shape, even at the end of transition. Figure 6(*c*) shows the turbulent zone profiles. All have a turbulent-like shape, and the last five stations show good agreement with the zero-pressure gradient law of the wall. The high FSTI suppresses the wake at all stations. Figure 7 illustrates the differences between the composite, nonturbulent, and turbulent profiles at Station 7, in the center of the transition zone. Distance from the wall is normalized on the composite flow $\delta_{99.5}$. Velocities in the turbulent zone are clearly higher in the near wall region due to higher levels of turbulent mixing. Also shown in Fig. 7 are low FSTI calculations for laminar and fully turbulent

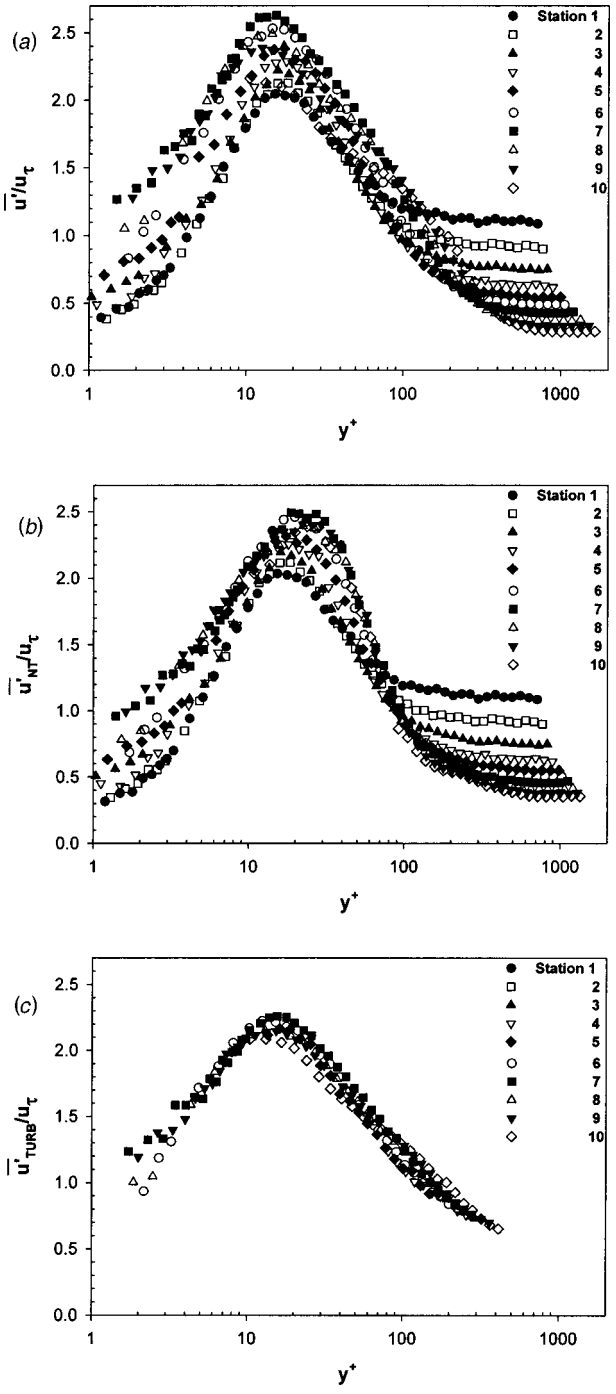

Fig. 11 Fluctuating streamwise velocity profiles in wall coordinates: (*a*) composite; (*b*) nonturbulent; (*c*) turbulent

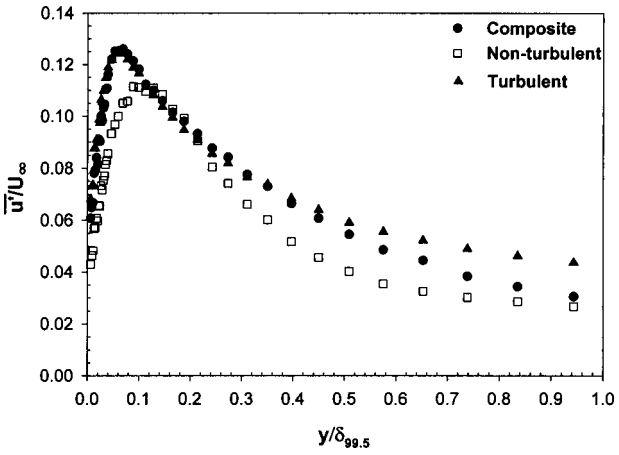

Fig. 12 Fluctuating streamwise velocity profile for Station 7, $\gamma_{pk}=56\%$

boundary layers with the same pressure gradient. The fully turbulent calculation was done with a mixing length model. The turbulent and nonturbulent zone profiles at all stations differ from the low FSTI calculations. Higher levels of transport lead to higher near wall mean velocities in the data than in the calculations. This is particularly true in the nonturbulent zone. The increased transport in the nonturbulent zone makes the differences between the turbulent and nonturbulent profiles less pronounced in the data than in the low FSTI calculations. At no point does the boundary layer behave as if it were laminar. Differences from laminar behavior have been reported in low FSTI transitional flows (e.g., [5], [15]) and attributed to the effect of the turbulent zone on the nonturbulent. In the present study, however, deviation from laminar behavior is seen even at Station 1, where the boundary layer is nearly all nonturbulent. The deviation from laminar behavior must be due to the high FSTI.

Boundary Layer Growth. Figure 8 shows the momentum thickness as a function of streamwise position. The composite boundary layer does not grow through the first five stations due to the strong acceleration. Momentum thickness increases at the downstream stations as the acceleration weakens and transition proceeds. In the nonturbulent zone, momentum thickness remains constant at all stations. The turbulent zone momentum thickness increases continuously, possibly due to turbulent entrainment at the edge of the boundary layer.

The shape factor, shown in Fig. 9, is an indicator of the state of the boundary layer with respect to transition. In the nonturbulent zone it drops only slightly from 2.0 to about 1.8. A low FSTI laminar boundary layer with the same pressure gradient would have a shape factor of 2.4. As shown in Fig. 7, the high FSTI enhances mixing and makes the nonturbulent zone appear less laminar-like. In the turbulent zone, H drops from about 1.5 to 1.35. The low FSTI fully turbulent calculation mentioned above resulted in H values about 10% higher than the experimental data. This suggests that the high FSTI promotes greater momentum transport in the turbulent zone, but the effect is not as great as in the nonturbulent zone.

Skin Friction Coefficients. Skin friction coefficients were computed from the mean velocity profiles and are shown in Fig. 10. Also shown for reference are the results from the low FSTI calculations. The skin friction coefficient is as much as 70% higher in the turbulent zone than in the nonturbulent zone. The composite C_f does not change much during transition, which if viewed alone, might suggest that there is little difference between the nonturbulent and turbulent zones. When viewed with the conditional sampling results, however, it is clear that the two zones

are quite different. In both zones the freestream turbulence results in C_f as much as 40% higher than the corresponding low FSTI calculation.

Fluctuating Velocity. Figure 11 shows $\overline{u'}$ profiles in wall coordinates. The composite flow data, shown in Fig. 11(*a*), are typical of transitional and turbulent boundary layers. The peak in $\overline{u'}/u_\tau$ occurs at $y^+ = 16$, and the magnitude of the peak is between 2 and 2.6. The peak is highest at Station 7, in the middle of transition, due in part to the unsteadiness associated with the switching between turbulent and nonturbulent states. The nonturbulent and turbulent zone data are shown in Figs. 11(*b*) and 11(*c*), respectively. In the turbulent zone the data from all stations collapse, showing self-similarity throughout the transition region. Figure 12 shows the $\overline{u'}$ profiles at Station 7, midway through transition. The peak in $\overline{u'}$ is closer to the wall in the turbulent zone, but the magnitudes of the peaks differ by only about 13% between the two zones.

Figure 13 shows $\overline{v'}$ profiles. The composite flow data are shown in Fig. 13(*a*). As expected for a high FSTI boundary layer, $\overline{v'}$ drops from a peak in the near wall region to a minimum, and then rises to the freestream value. The minimum is indicative of a damping of the freestream effect by the wall. Near the wall, there is not much change in $\overline{v'}/u_\tau$ for the first three stations. As transition begins, $\overline{v'}/u_\tau$ rises at Stations 4 and 5. Between Stations 6 and 10 there is little change. In comparison to the $\overline{u'}$ profiles of Fig. 11, $\overline{v'}$ is lower in magnitude and shows more change through the transition region. Far from the wall, normalized $\overline{v'}$ drops in the streamwise direction due to the increasing value of u_τ. The dimensional value of $\overline{v'}$ in the freestream remains essentially constant at 0.4 m/s at all stations. The nonturbulent and turbulent zone data are shown in Figs. 13(*b*) and 13(*c*). As with $\overline{u'}$, the turbulent zone profiles collapse. Figure 14 shows the $\overline{v'}$ profiles at Station 7. In contrast to the $\overline{u'}$ profiles of Fig. 12, which showed similar magnitude in the turbulent and nonturbulent zones, the $\overline{v'}$ magnitude is nearly twice as high in the turbulent zone as in the nonturbulent. Volino [17] found that much of the unsteadiness in u is low-frequency unsteadiness induced by the freestream and common to both zones. When freestream eddies buffet the boundary layer and push higher speed fluid toward the wall, the effect is an increase in u, particularly near the wall where $\partial U/\partial y$ is large. This effect is common to both the nonturbulent and turbulent zones and is not dependent on turbulence produced near the wall. It explains the similarity between the turbulent and nonturbulent $\overline{u'}$ behavior. There is no similar effect on $\overline{v'}$, so the $\overline{v'}$ fluctuations are more closely related to turbulence and eddy transport in the boundary layer, and greater differences exist between the turbulent and nonturbulent $\overline{v'}$.

Turbulent Shear Stress. Profiles of the turbulent shear stress are shown in Fig. 15 in wall coordinates. Similar to $\overline{v'}/u_\tau$ in Fig. 13(*a*), there is little change in the composite profiles in Fig. 15(*a*) for the first three stations. As transition begins, the dimensionless shear stress rises. In the nonturbulent zone (Fig. 15(*b*)) $-\overline{u'v'}$ values are low. In the turbulent zone, Fig. 15(*c*) shows that the data from beginning to end of transition all collapse onto a single line. To compare the turbulent and nonturbulent $-\overline{u'v'}$ directly, Fig. 16 shows the Station 7 profiles. In contrast to $\overline{u'}$, which had similar magnitude in the two zones, $-\overline{u'v'}$ is much higher in the

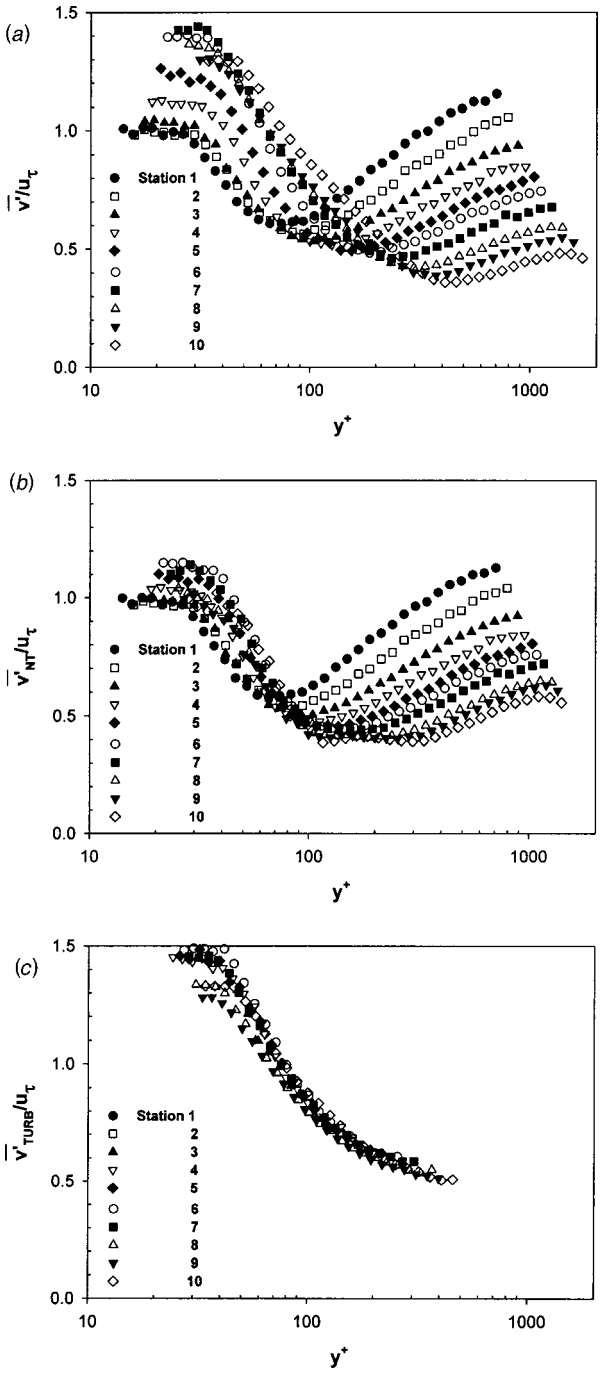

Fig. 13 Fluctuating wall-normal velocity profiles in wall coordinates: (*a*) composite; (*b*) nonturbulent; (*c*) turbulent

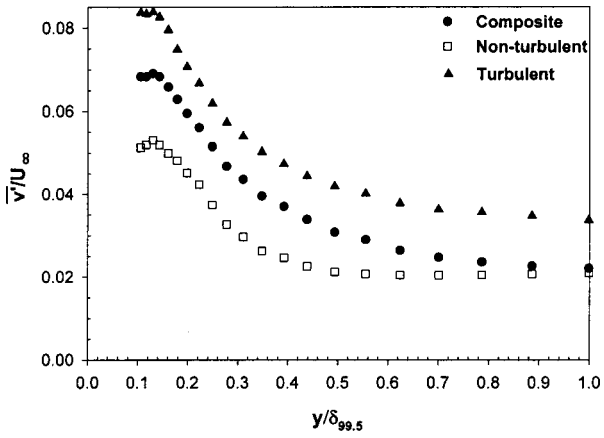

Fig. 14 Fluctuating wall-normal velocity profile for Station 7, γ_{pk}=56%

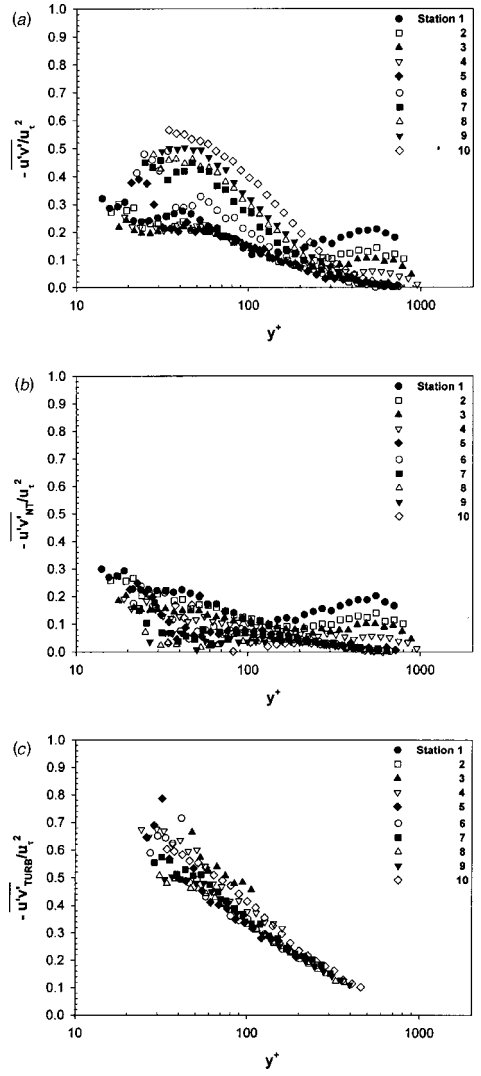

Fig. 15 Reynolds shear stress profiles in wall coordinates: (*a*) composite; (*b*) nonturbulent; (*c*) turbulent

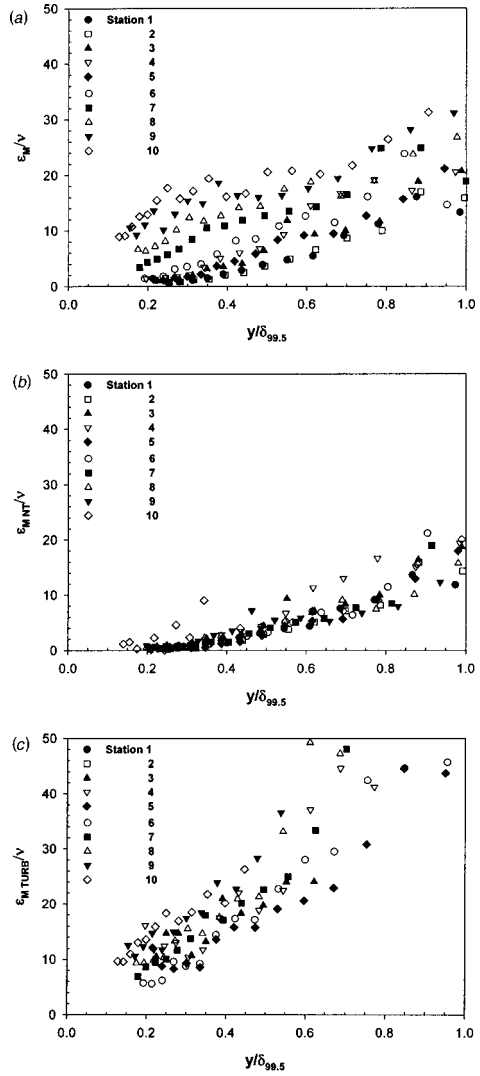

Fig. 17 Eddy viscosity profiles: (*a*) composite; (*b*) nonturbulent; (*c*) turbulent

turbulent zone. The nonturbulent $-\overline{u'v'}$ is not zero, however, indicating some eddy transport of momentum even when the boundary layer is non-turbulent. This may explain the deviation of the nonturbulent mean velocity profiles from laminar predictions and the enhancement of the skin friction above laminar values shown in Figs. 7 and 10.

The collapse of the turbulent zone data in Fig. 15(*c*), also seen in $\overline{u'}$ and $\overline{v'}$ in Figs. 11(*c*) and 13(*c*), indicates considerable similarity within the turbulent zone. The turbulence contained within the turbulent spots in the upstream part of transition (where the intermittency is low and the spots occupy only a small fraction of the total flow) appears to be very similar to the turbulence in the nearly fully turbulent region downstream. This similarity may simplify modeling of the turbulent zone. Although the collapse of the data in the coordinates of Figs. 11(*b*), 13(*b*), and 15(*b*) is not quite so good, similar arguments can be made concerning the self-similarity of the nonturbulent zone.

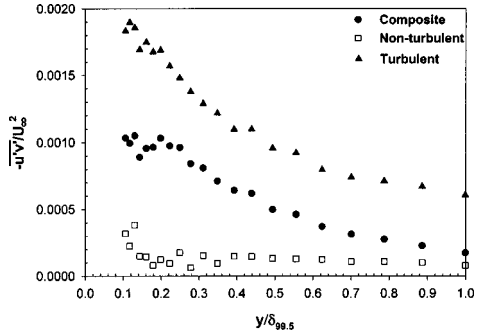

Fig. 16 Reynolds shear stress profile for Station 7, γ_{pk}=56%

Profiles of the eddy viscosity are shown in Fig. 17. The composite profiles in Fig. 17(*a*) show that ε_M increases in the streamwise direction as the transition proceeds. Comparison of the nonturbulent and turbulent zone profiles in Figs. 17(*b*) and 17(*c*) shows that the eddy viscosity is three to four times higher in the turbulent zone. While the difference between the two zones is clear, Fig. 17(*b*) again shows that there is significant eddy transport in the nonturbulent zone.

Conclusions

Conditional sampling was successfully performed on experimental data from a transitional boundary layer subject to high freestream turbulence and strong acceleration. Intermittency func-

tions based on the instantaneous streamwise velocity and the instantaneous turbulent shear stress agreed well and produced essentially equal conditional sampling results.

Mean velocity profiles differed significantly between the turbulent and nonturbulent zones, and skin friction coefficients in the turbulent zone were as much as 70% higher than in the nonturbulent zone. The $\overline{u'}$ fluctuation levels did not differ greatly between the turbulent and nonturbulent zones, but $\overline{v'}$ and the turbulent shear stress were significantly higher in the turbulent zone. Within each zone, considerable self-similarity was observed in all turbulence quantities from beginning to end of transition, particularly in the turbulent zone. The differences between the two zones and the similarity within each zone suggest the importance of properly modeling the transition process in boundary layer prediction and support arguments for the development of intermittency based models.

Although the turbulent shear stress was higher in the turbulent zone, nonturbulent zone eddy transport was still significant. In both zones there was significant deviation from low FSTI predictions.

Acknowledgments

Bill Beaver of the Technical Support Department at the U.S. Naval Academy constructed the test section. One of the authors (MPS) was supported by the Office of Naval Research as a postdoctoral fellow during the period of this work.

Nomenclature

C_f = $\tau_w/(\rho U_\infty^2/2)$, skin friction coefficient
FSTI = freestream turbulence intensity
f = frequency
$f(\gamma_{pk})$ = function of intermittency, Eq. (8)
H = δ^*/θ, shape factor
K = $(\nu/U_\infty^2)(dU_\infty/dx)$, acceleration parameter
$\hat{n}$ = dimensionless turbulent spot production rate
Re_x = $U_\infty x/\nu$, Reynolds number
Re_θ = momentum thickness Reynolds number
t = time
U = time-averaged local streamwise velocity
U_m = adjusted local velocity, Eq. (3)
U_∞ = average freestream velocity in transition region
u = instantaneous streamwise velocity
U^+ = U/u_τ, local mean streamwise velocity in wall coordinates
u' = instantaneous streamwise fluctuating velocity
$\overline{u'}$ = rms streamwise fluctuating velocity, $\sqrt{\overline{u'^2}}$
u_τ = τ_w/ρ, friction velocity

$-u'v'$ = instantaneous turbulent shear stress

$-\overline{u'v'}$ = time averaged turbulent shear stress
$\overline{v'}$ = rms cross-stream fluctuating velocity, $\sqrt{\overline{v'^2}}$
x = streamwise coordinate, distance from leading edge
y = cross-stream coordinate, distance from wall
y^+ = yu_τ/ν, distance from wall-in-wall coordinates
$\delta_{99.5}$ = 99.5% boundary layer thickness
δ^* = displacement thickness
ε_M = $-\overline{u'v'}/(dU/dy)$, eddy viscosity
Γ = intermittency function
γ = intermittency, time average of Γ (fraction flow is turbulent)
γ_{pk} = peak intermittency in profile
ν = kinematic viscosity
ρ = density
θ = momentum thickness
σ = turbulent spot propagation parameter
τ_w = wall shear stress

Subscripts

HP = high pass
LP = low pass
s = transition start
e = transition end
u = intermittency based on streamwise velocity
uv = intermittency based on turbulent shear stress
∞ = local freestream condition
1,2,3 = intermediate steps in construction of intermittency function
NT = nonturbulent zone
TURB = turbulent zone

References

[1] Mayle, R. E., 1991, "The Role of Laminar-Turbulent Transition in Gas Turbine Engines," ASME J. Turbomach., **113**, pp. 509–537.
[2] Halstead, D. E., Wisler, D. C., Okiishi, T. H., Walker, G. J., Hodson, H. P., and Shin, H.-W., 1997, "Boundary Layer Development in Axial Compressors and Turbines: Part 3 of 4—LP Turbines," ASME J. Turbomach., **119**, pp. 225–237.
[3] Blair, M. F., 1983, "Influence of Free-Stream Turbulence on Turbulent Boundary Layer Heat Transfer and Mean Profile Development: Part 1—Experimental Data," ASME J. Turbomach., **105**, pp. 33–40.
[4] Sohn, K. H., and Reshotko, E., 1991, "Experimental Study of Boundary Layer Transition with Elevated Freestream Turbulence on a Heated Flat Plate," NASA CR 187068.
[5] Kim, J., Simon, T. W., and Kestoras, M., 1994, "Fluid Mechanics and Heat Transfer Measurements in Transitional Boundary Layers Conditionally Sampled on Intermittency," ASME J. Turbomach., **116**, pp. 405–416.
[6] Blair, M. F., 1992, "Boundary Layer Transition in Accelerating Flows With Intense Freestream Turbulence: Part 1—Disturbances Upstream of Transition Onset; Part 2—The Zone of Intermittent Turbulence," ASME J. Fluids Eng., **114**, pp. 313–332.
[7] Volino, R. J., and Simon, T. W., 1997, "Boundary Layer Transition Under High Free-Stream Turbulence and Strong Acceleration Conditions: Part 1—Mean Flow Results; Part 2—Turbulent Transport Results," ASME J. Heat Transfer, **119**, pp. 420–432.
[8] Volino, R. J., and Simon, T. W., 2000, "Spectral Measurements in Transitional Boundary Layers on a Concave Wall Under High and Low Free-Stream Turbulence," ASME J. Turbomach., **122**, pp. 450–457.
[9] Volino, R. J., and Simon, T. W., 1995, "Measurements in Transitional Boundary Layers under High Free-Stream Turbulence and Strong Acceleration Conditions," NASA CR 198413.
[10] Volino, R. J., 1998, "A New Model for Free-Stream Turbulence Effects on Boundary Layers," ASME J. Turbomach., **120**, pp. 613–620.
[11] Steelant, J., and Dick, E., 1996, "Modeling of Bypass Transition with Conditioned Navier-Stokes Equations Coupled to an Intermittency Transport Equation," Int. J. Numer. Methods Fluids, **23**, pp. 193–220.
[12] Suzen, Y. B., and Huang, P. G., 2000, "Modeling of Flow Transition Using an Intermittency Transport Equation," ASME J. Fluids Eng., **122**, pp. 273–284.
[13] Solomon, W. J., Walker, G. J., and Gostelow, J. P., 1995, "Transition Length Prediction for Flows with Rapidly Changing Pressure Gradients," ASME Paper No. 95-GT-241.
[14] Kuan, C. L., and Wang, T., 1990, "Investigation of the Intermittent Behavior of a Transitional Boundary Layer Using a Conditional Averaging Technique," Exp. Therm. Fluid Sci., **3**, pp. 157–170.
[15] Wang, T., and Feller, F. J., 1999, "Intermittent Flow and Thermal Structures of Accelerating Transitional Boundary Layers, Part 1—Mean Quantities; Part 2—Fluctuation Quantities," ASME J. Turbomach., **121**, pp. 98–112.
[16] Wang, T., and Zhou, D., 1998, "Conditionally Sampled Flow and Thermal Behavior of a Transitional Boundary Layer at Elevated Free-Stream Turbulence," Int. J. Heat Fluid Flow, **19**, pp. 348–357.
[17] Volino, R. J., 1998, "Wavelet Analysis of Transitional Flow Data Under High Free-Stream Turbulence Conditions," ASME Paper No. 98-GT-289.
[18] Schultz, M. P., and Volino, R. J., 2003, "Effects of Concave Curvature on Boundary Layer Transition Under High Free-Stream Turbulence Conditions," ASME J. Fluids Eng., **125**, pp. 18–27.
[19] Wills, J. A. B., 1962, "The Correction of Hot-Wire Readings for Proximity to a Solid Boundary," J. Fluid Mech., **12**, pp. 388–396.
[20] Volino, R. J., and Simon, T. W., 1997, "Velocity and Temperature Profiles in Turbulent Boundary Layer Flows Experiencing Streamwise Pressure Gradients," ASME J. Heat Transfer, **119**, pp. 433–439.
[21] Keller, F. J., and Wang, T., 1995, "Effects of Criterion Functions on Intermittency in Heated Transitional Boundary Layers With and Without Streamwise Acceleration," ASME J. Turbomach., **117**, pp. 154–165.
[22] Solomon, W. J., 1996, "Unsteady Boundary Layer Transition on Axial Compressor Blades," Ph.D. thesis, University of Tasmania, Hobart, Tasmania, Australia.
[23] Volino, R. J., and Hultgren, L. S., 2000, "Measurements in Separated and Transitional Boundary Layers Under Low-Pressure Turbine Airfoil Conditions," ASME J. Turbomach., **123**, pp. 189–197.

[24] Johnson, M. W., 1994, ''A Bypass Transition Model for Boundary Layers,'' ASME J. Turbomach., **116**, pp. 759–764.
[25] Jones, W. P., and Launder, B. E., 1972, ''Some Properties of Sink-Flow Turbulent Boundary Layers,'' J. Fluid Mech., **56**, pp. 337–351.
[26] Narasimha, R., 1985, ''The Laminar-Turbulent Transition Zone in the Boundary Layer,'' Prog. Aerosp. Sci., **22**, pp. 29–80.
[27] Volino, R. J., and Simon, T. W., 1995, ''Bypass Transition in Boundary Layers Including Curvature and Favorable Pressure Gradient Effects,'' ASME J. Turbomach., **117**, pp. 166–174.
[28] Dhawan, S., and Narasimha, R., 1958, ''Some Properties of Boundary Layer Flow During the Transition from Laminar to Turbulent Motion,'' J. Fluid Mech., **3**, pp. 418–436.